Vimentin Filaments Support Extension of Tubulin-Based Microtentacles in Detached Breast Tumor Cells

Rebecca A. Whipple,[1] Eric M. Balzer,[1,2] Edward H. Cho,[1,2] Michael A. Matrone,[1,2] Jennifer R. Yoon,[1,2] and Stuart S. Martin[1,2]

[1]University of Maryland School of Medicine, Marlene and Stewart Greenebaum Cancer Center, Department of Physiology and [2]Graduate Program in Life Sciences Baltimore, Maryland

Abstract

Solid tumor metastasis often involves detachment of epithelial carcinoma cells into the vasculature or lymphatics. However, most studies of cytoskeletal rearrangement in solid tumors focus on attached cells. In this study, we report for the first time that human breast tumor cells produce unique tubulin-based protrusions when detached from extracellular matrix. Tumor cell lines of high metastatic potential show significantly increased extension and frequency of microtubule protrusions, which we have termed tubulin *microtentacles*. Our previous studies in nontumorigenic mammary epithelial cells showed that such detachment-induced microtentacles are enriched in detyrosinated α-tubulin. However, amounts of detyrosinated tubulin were similar in breast tumor cell lines despite varying microtentacle levels. Because detyrosinated α-tubulin associates strongly with intermediate filament proteins, we examined the contribution of cytokeratin and vimentin filaments to tumor cell microtentacles. Increased microtentacle frequency and extension correlated strongly with loss of cytokeratin expression and up-regulation of vimentin, as is often observed during tumor progression. Moreover, vimentin filaments coaligned with microtentacles, whereas cytokeratin did not. Disruption of vimentin with PP1/PP2A-specific inhibitors significantly reduced microtentacles and inhibited cell reattachment to extracellular matrix. Furthermore, expression of a dominant-negative vimentin mutant disrupted endogenous vimentin filaments and significantly reduced microtentacles, providing specific genetic evidence that vimentin supports microtentacles. Our results define a novel model in which coordination of vimentin and detyrosinated microtubules provides structural support for the extensive microtentacles observed in detached tumor cells and a possible mechanism to promote successful metastatic spread. [Cancer Res 2008;68(14):5678–88]

Introduction

Successful tumor cell colonization in distant tissues depends on overcoming the selective pressures that are imposed on tumor cells during metastasis (1). Such pressures often select for signaling pathways that support tumor cell survival, motility, invasion, and proliferation after release from the primary tumor site (2–4). Under normal conditions, detachment and dissemination of epithelial carcinoma cells into the microvasculature result in apoptosis or necrosis by shearing forces in narrow capillaries (5, 6). However, metastatic tumor cells are able to persist through adapted signaling pathways and can tolerate the morphologic alterations in cell shape, plasticity, and deformation that are necessary to readhere and extravasate into distant sites (7–9).

Growing evidence has necessitated a reevaluation of the functional implications that stable microtubules have in tumor metastasis. We previously reported observations of extensive and motile microtubule-enriched membrane protrusions in detached mouse and human mammary epithelial cells, which promote cell-cell adherence and reattachment to uncoated and extracellular matrix (ECM)–coated culture surfaces (10). These protrusions are mechanistically distinct from actin-based invadopodia, filopodia, and cilia and have been termed tubulin *microtentacles* (10). Microtubule-destabilizing agents significantly reduced the frequency with which microtentacles were observed and impaired both cell-cell interaction and reattachment of cells to surfaces. Interestingly, microtubule-destabilizing drugs prevent circulating colon carcinoma cells from attaching to the microvascular endothelium *in vivo*, although the precise mechanism is currently unclear (11). Strikingly, actin depolymerization significantly increases binding of circulating tumor cells to the vascular endothelium (11) and also strongly promotes the extension of tubulin microtentacles (10).

The stability of microtubules is influenced by the reversible posttranslational cleavage of the COOH terminal tyrosine of full-length α-tubulin, which is termed tyrosinated tubulin (Tyr-tubulin; ref. 12). Through the action of a yet-unidentifed carboxypeptidase, this tyrosine can be removed rapidly *in vivo*, exposing a COOH terminal glutamic acid residue and forming detyrosinated α-tubulin (Glu-tubulin; ref. 13). Importantly, poor patient prognosis correlates with elevated levels of Glu-tubulin in breast tumors (14), neuroblastomas (15), and prostate tumors (16), but the mechanism by which increased Glu-tubulin affects tumor progression is currently unknown. We have shown that Glu-tubulin levels significantly increase after epithelial cell detachment and detachment-induced microtentacles are enriched in Glu-tubulin (10). Cytoplasmic microtubules enriched in Glu-tubulin persist for as long as 16 hours, whereas microtubules enriched in Tyr-tubulin generally turn over within minutes (13). However, detyrosination does not directly stabilize tubulin polymers, as Tyr-tubulin and Glu-tubulin polymerize identically *in vitro* (17). Rather, detyrosinated microtubules associate preferentially with more resilient cytoskeletal components (18), such as the vimentin intermediate filament (IF). This candidate type III IF protein displays anterograde movement toward the plus-ends of microtubules (19). Light and electron microscopy also show that IFs and microtubules run parallel in close proximity (20).

Given our recent findings that nontumorigenic mammary epithelial cells display tubulin microtentacles following detachment

Note: Supplementary data for this article are available at Cancer Research Online (http://cancerres.aacrjournals.org/).

Requests for reprints: Stuart S. Martin, Bressler Building, Room 10-29, 655 W. Baltimore Street, Baltimore, MD 21201. Phone: 410-706-6601; Fax: 410-706-6600; E-mail: ssmartin@som.umaryland.edu.

doi:10.1158/0008-5472.CAN-07-6589

(10), we explored the occurrence of microtubule-based microtentacles and microtubule-associated cytoskeletal proteins in a panel of human breast carcinoma cells. We report for the first time that vimentin-expressing invasive breast carcinomas display a comparatively higher frequency of tubulin microtentacles following detachment than non–vimentin-expressing, noninvasive cell lines. Microtentacle preservation following detachment indicates that vimentin coaligns with Glu-tubulin in microtentacles, whereas cytokeratin does not. Time-lapse video shows that membrane microtentacles are rapidly disrupted by treatment with PP1/PP2A inhibitors that disassemble vimentin, decreasing microtentacle frequency and impairing reattachment of vimentin-expressing tumor cells. Finally, a dominant-negative vimentin mutant disrupts endogenous vimentin filaments and reduces microtentacles, demonstrating a direct role for vimentin assembly in the mechanism underlying breast tumor microtentacles.

Materials and Methods

Cell culture. MCF10A human mammary epithelial cells of low passage were grown in DMEM/F12 (Life Technologies) supplemented with 5% horse serum, insulin (5 μg/mL), epidermal growth factor (20 ng/mL), hydrocortisone (500 ng/mL). SkBr3, Bt20, MDA-468, Hs578t, and MDA-MB-436 were maintained in DMEM (Life Technologies), whereas ZR75-1 and HCC1395 were maintained in RPMI (Life Technologies), both supplemented with 10% bovine calf serum at 37°C in 5% CO_2. MDA-MB-157 were maintained in L-15 (Life Technologies) supplemented with 10% fetal bovine serum (FBS) at 37°C without CO_2. TIB-131 hybridoma cells that secrete a PAN-IF antibody (21) were maintained in DMEM supplemented with 10% hybridoma–qualified FBS, sodium pyruvate (1.0 mM) at 37°C in 10% CO_2. Sequential adaptation in hybridoma serum-free media (Life Technologies) was used to subculture cells to minimal serum level for antibody isolation. All cell lines were obtained by American Type Culture Collection, and all media were supplemented with penicillin-streptomycin (100 μg/mL each) and L-glutamine (2 mM).

Vimentin expression constructs and transfection. Human vimentin was cloned into the NH_2 terminal eGFP pReceiver-M29 expression vector (Genecopoeia). The truncated vimentin was generated by restriction at the internal vimentin *Xho*I site (position 403) and religating the 5′ overhang with a flanking *Xho*I site at the COOH terminal multiple cloning site. Both the full-length and truncated vimentin were separated on a gel and sequenced.

Transient transfections of membrane targeted AcGFP1-Mem (Clontech) and CMV-pmRFP-Mem (kindly provided by Georges Luftalla and previously described; ref. 22) were used to visualize and score membrane microtentacles in suspended cells via fluorescent microscopy. Cotransfections were performed with the pmRFP-Mem and the N-GFP vimentin constructs in a 1:1 DNA ratio. MCF10A, SkBr3, Bt20, and MDA-MB-157 cells were transfected according to manufacturer's protocol with FuGENEHD transfection reagent (Roche) using a complex ratio of 3 μL of FuGENEHD to 2 μg of DNA. ZR75-1, HCC1395, MDA-468, Hs578t, and MDA-MB-436 cells were transfected with Exgen500 (Fermentas) using complex ratio of 5.3 μL of Exgen500 to 2 μg of DNA.

Validated double-stranded small interfering RNA (siRNA) oligonucleotides for human vimentin (5′-CTGGCACGTCTTGACCTTGAA-3′) and a conjugated Alexa Fluor 488 nonsilencing control were purchased from Qiagen. MDA-MB-436 cells were transfected with HiPerfect (Qiagen) with 5 nM of siRNA. Western blot analysis and immunofluorescence was performed 4, 5, and 6 d posttransfection. For microtentacle scoring at 6 d post–siRNA transfection, MDA-MB-436 cells were split 4 d posttransfection into optimal confluency conditions for GFP-Mem transfection.

Live cell imaging and membrane microtentacle scoring. Cells were trypsinzed at ~80% confluency after 24 h expression and resuspended in serum/phenol red (PR)–free media over ultralow attachment plates in the presence or absence of 5 μM Latrunculin-A (LA; BioMol) for 1 h. For microtentacle scoring involving phosphatase inhibitor treatment, MCF10A and MDA-MB-436 were pretreated with either 1 μM okadiac acid (OKA; Sigma) or 5 nM Calyculin-A (Cal-A; Chemicon) in serum-containing media for 1 h and resuspended in serum/PR-free media in the respective phosphatase inhibitor with or without 5 μM LA.

Single cells were scored blindly for microtentacles at 1 h in suspension, and GFP^+ cells were photographed by fluorescent microscopy. Cells with two or more microtentacles extending greater than the radius of the cell body were scored as positive. Populations of 100 or more GFP^+ cells were counted for each trial. Live and fixed cell images were collected using an Olympus CKX41 inverted fluorescent microscope equipped with the Olympus F-View II 12-bit CCD digital camera system and Olympus MicroSuite Five imaging software. Movies of detached cells were captured at one frame every 2 s and shown with a 5× acceleration.

Differential interference contrast (DIC) images of MDA-MB-436 cells suspended over 35-mm glass-bottomed dishes (MatTek) were acquired using a Zeiss Axiovert 200M motorized microscope equipped with a stage-enclosed incubation system (Incubator XL-3, PeCon). Cells were incubated at 37°C for 10 min to allow for transient attachment to anchor cells. Cells that displayed active membrane microtentacles were selected for imaging. Selected cells were imaged over time pretreatment and posttreament with 1 μM OKA or 5 nM Cal-A. Three-dimensional image stacks were acquired every 3 min for up to 45 min. Zeiss Axiovision software was used for image acquisition and cropping.

Immunofluorescence. To determine cytoskeletal composition of microtentacles observed in suspension, MCF10A and MDA-MB-436 cells were suspended in serum/PR-free media for 30 min in the presence or absence of 5 μM LA. Cells were then fixed in suspension (0.5% glutaraldehyde, 5 min) and gently spun (200 rpm, 5 min) onto glass coverslips coated with 1% poly(ethyleneimine) (PEI) solution. Fixative-containing media was aspirated, and autofluorescene was quenched using 1 mg/mL sodium borohydride solution. For attached cell experiments, MCF10A and MDA-MB-436 on glass coverslips were treated with either 1 μM OKA or 5 nM Cal-A in serum-free media for 1 h at ~80% confluency. Cells were fixed in 3.7% formaldehyde/PBS (10 min, room temperature).

Fixed cells were permeablized (0.25% Triton X-100/PBS, 10 min), and blocked for 1 h [PBS/5% bovine serum albumin (BSA)/0.5% NP40]. Immunostaining was performed using mouse monoclonal antibodies vimentin clone V9 (1:1,000; Zymed) and PAN cytokeratin clone AE1/AE3 (1:1,000; Zymed) and rabbit polyclonal antidetyrosinated tubulin (Glu; 1:500; Chemicon). Primary incubation was performed overnight at 4°C (PBS/2% BSA/0.5% NP40). Anti-IgG antibodies conjugated to Alexa-594 and Alexa-488 (1:1,000; Molecular Probes) were used for secondary detection and Hoescht 33342 (1:5,000; Sigma) was used for nuclear staining.

Western blot. The panel of confluent, untreated cells or, specifically, MCF10A and MDA-MB-436 treated in serum/PR-free media at various time points in 1 μM OKA, 5 nM Cal-A, or 30 μg/mL cycloheximide were harvested in ice-cold radioimmunoprecipitation assay lysis buffer [50 mM Tris-HCl (pH 8.0), 150 mM NaCl, 1% NP40, 0.5% sodium deoxycholate, 0.1% SDS, 1 mM phenylmethylsulfonyl fluoride, 1% protease inhibitor cocktail (Sigma, P2714)]. Lysates were subjected to high-speed centrifugation (14,000 rpm × 10 min), and protein concentration was measured using a Lowry-based assay (Bio-Rad). Total protein (20 μg) was separated by SDS-PAGE on 10% polyacrylamide gels and then transferred to Immuno-Blot polyvinylidene difluoride membranes (Bio-Rad). Membranes were blocked in 5% milk in TBS with 0.1% Tween for 1 h at room temperature followed by an overnight incubation at 4°C in monoclonal α-tubulin (1:1,000; Sigma Chemical), PAN cytokeratin clone AE1/AE3 (1:1,000; Zymed), and polyclonal detyrosinated tubulin (1:1,000; Chemicon), vimentin (C-20, Santa Cruz Biotechnology; 1:1,000), vimentin (H-84, Santa Cruz Biotechnology; 1:1,000), and poly (ADP-ribose) polymerase (PARP; H-250, Santa Cruz Biotechnology; 1:1,000) in 2.5% milk in TBST. Monoclonal PAN-IF isolated from TIB-131 hybridoma cells (1:250) was incubated overnight in 5% milk in TBST. Secondary antibodies to IgG conjugated to horseradish peroxidase were used (1:5,000; GE Healthcare) and visualized using ECL+ chemiluminescent detection kit.

Attachment assay. MCF10A and MDA-MB-436 cells were grown to confluency in six-well plates and pretreated in either 1 μM OKA or 5 nM Cal-A in serum-containing media for 1 h. Media and subsequent PBS wash were

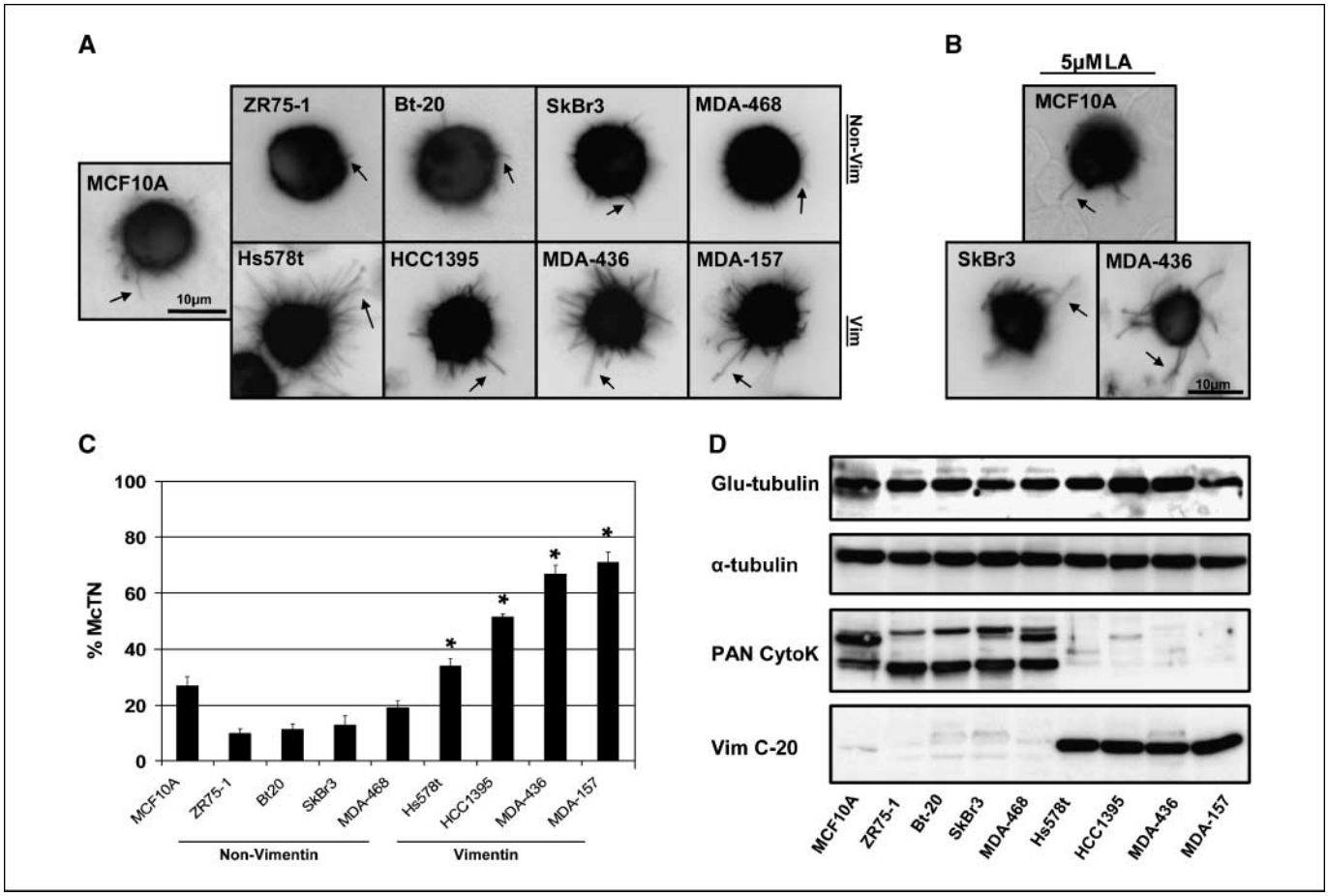

Figure 1. Microtentacles in detached human breast tumor cell lines. *A,* human mammary epithelial cells (MCF10A) and breast tumor cell lines transfected with GFP-membrane (*GFP-Mem*) and plated over low-attachment wells display morphologically different extensive membrane microtentacles 30 min following detachment (*black arrows*). Invasive cell lines (HCC1395, Hs578t, MDA-MB-436, MDA-MB-157) exhibit long, flexible microtentacles, whereas noninvasive lines (MCF10A, ZR75-1, Bt-20, SkBr3, MDA-MB-468) display short, rigid microtentacles. *B,* treatment with actin-depolymerizing agent LA (5 μM) enhanced the flexibility and length of observed microtentacles. *C,* populations of live, suspended cells were scored blindly for two or more microtentacles longer than the cell radius. *Columns,* mean for three experiments, in which at least 100 single GFP-Mem$^+$ cells were counted; *bars,* SD. Vimentin-expressing, invasive cell lines had a statistically significant higher frequency than non–vimentin-expressing, noninvasive cell lines ($P < 0.05$, *t* test, *black asterisks*). *D,* Western blot expression profile of Glu-tubulin, α-tubulin, PAN-cytokeratin, and vimentin indicates that cells with higher microtentacle frequencies express elevated vimentin and lower cytokeratin, and Glu-tubulin remains largely unchanged.

collected to recover all cells. Cells were trypsinized and resuspended in serum-containing media, collected into respective tube, and pelleted by centrifugation (1,000 rpm × 5 min). Media were aspirated from pellet, and cells were gently triturated in fresh serum–containing media containing 1 μM OKA or 5 nM Cal-A. Cells plated in triplicate in 96-well clear-bottomed uncoated or laminin-coated (BD Biosciences) plates (the attachment plate). Cells were allowed to attach for duration of 15 min, 45 min, 1.5 h, 3 h, 4 h, 6 h, and 24 h, at which point the media was collected into a fresh 96-well uncoated plate (the collection plate). The attachment plate was washed gently with fresh serum–containing growth media without PR, and the wash was combined into the collection plate. Fresh growth media was replaced at each time point on the original attachment plate. After 24 h, a 2,3-bis[2-methoxy-4-nitro-5-sulfophenyl]-2H-tetrazolium-5-carboxanilide inner salt (XTT) viability assay was performed on both the attachment and collection plate to quantitatively determine the percentage of total number of cells plated that had attached at each time point. Absorbance was measured using a Biotek Synergy HT Multidetection Microplate Reader at 450 nm. All values are shown as mean ± SD of triplicate samples.

Results

Human mammary carcinoma cell lines display morphologically different membrane microtentacles following detachment. We compared the tubulin microtentacles observed in the nontumorigenic MCF10A human mammary epithelial cell line (10) with those in a panel of human breast tumor cell lines. GFP-Mem$^+$ cell lines were detached and suspended over ultralow attachment plates in media deprived of serum and growth factors. Grayscale images collected with fluorescence microscopy were subsequently color inverted for better visualization contrast. Detachment of invasive breast tumor cell lines Hs578t, HCC1395, MDA-MB-436, and MDA-MB-157 produced unusually long, semiflexible, and motile microtentacles compared with noninvasive MCF10A, ZR-75-1, Bt-20, SkBr3, and MDA-MB-468 lines, which display relatively short, rigid, and semimotile microtentacles (Fig. 1*A* and Supplementary Movies S1–S3). Our previous research has shown that inhibiting actin polymerization with LA (5 μM) enhances microtentacle frequency, motility, and length in both human and mouse mammary epithelial cells following detachment (10). LA similarly increases the length, flexibility, and motility of microtentacles in breast tumor cells (Fig. 1*B* and Supplementary Movies S4–S6). However, the invasive breast tumor cell lines were clearly able to form dynamic and flexible microtentacles even in the absence of LA treatment. Blinded scoring of microtentacle

frequencies (described in Materials and Methods) was conducted in live cells after 30 min to 1 h in suspension for each of four independent trials. Invasive breast tumor cell lines (Hs578t, HCC1395, MDA-MB-436, and MDA-MB-157) all displayed significantly higher microtentacle frequencies ($P < 0.05$, t test) than the noninvasive breast tumor cell lines (Zr-75-1, Bt-20, SkBr3, and MDA-MB-468) or nontumorigenic MCF10A cells (Fig. 1*C*). Microtentacles in both untreated and LA-treated human carcinoma cells can persist at least 48 hours (data not shown), whereas MCF10A cells are highly fragmented by late-stage apoptosis after 48 hours of detachment (10).

Vimentin-expressing cell lines have more frequent and extensive tubulin microtentacles. While we previously reported that microtentacles are enriched in detyrosinated (Glu) α-tubulin (10), we did not observe significant differences in Glu-tubulin modification or total cellular expression of α-tubulin in the panel of breast tumor cell lines (Fig. 1*D*). These data indicated that Glu-tubulin alone may not account for such distinct morphologies and increased microtentacle frequency in these cell lines. Because microtubules interact with IFs, we examined cytokeratin and vimentin expression in these cell lines. Western blot analysis (Fig. 1*D*) and indirect immunofluorescence (data not shown) confirmed that noninvasive epithelioid cell lines ZR-75-1, Bt-20, SkBr3, and MDA-MB-468 homogeneously expressed cytokeratin, and not vimentin, whereas moderate to highly invasive fibroblastioid-like cell lines Hs578t, HCC1395, MDA-MB-436, and MDA-MB-157 cells homogeneously expressed vimentin, and not cytokeratin. Nontumorigenic human mammary epithelial cell line MCF10A displayed heterogeneous expression of both vimentin and cytokeratin, with cytokeratin as the dominating intermediate filament in cell monolayers and pronounced vimentin expression at monolayer edges (data not shown). Expression of vimentin is much higher in breast tumor cells which display long and numerous microtentacles, whereas cytokeratin expression predominated in those cell lines that displayed fewer and shorter microtentacles (Fig. 1*D*).

Vimentin extends into microtentacles. Given the correlation of vimentin expression in those cells that exhibit more extensive and frequent microtentacles, we examined intermediate filament localization with indirect immunofluorescence, finding that vimentin, and not cytokeratin, extends into microtentacles (Fig. 2). MCF10A and MDA-MB-436 were used for this and all subsequent experiments due to the extensive microtentacles of the invasive

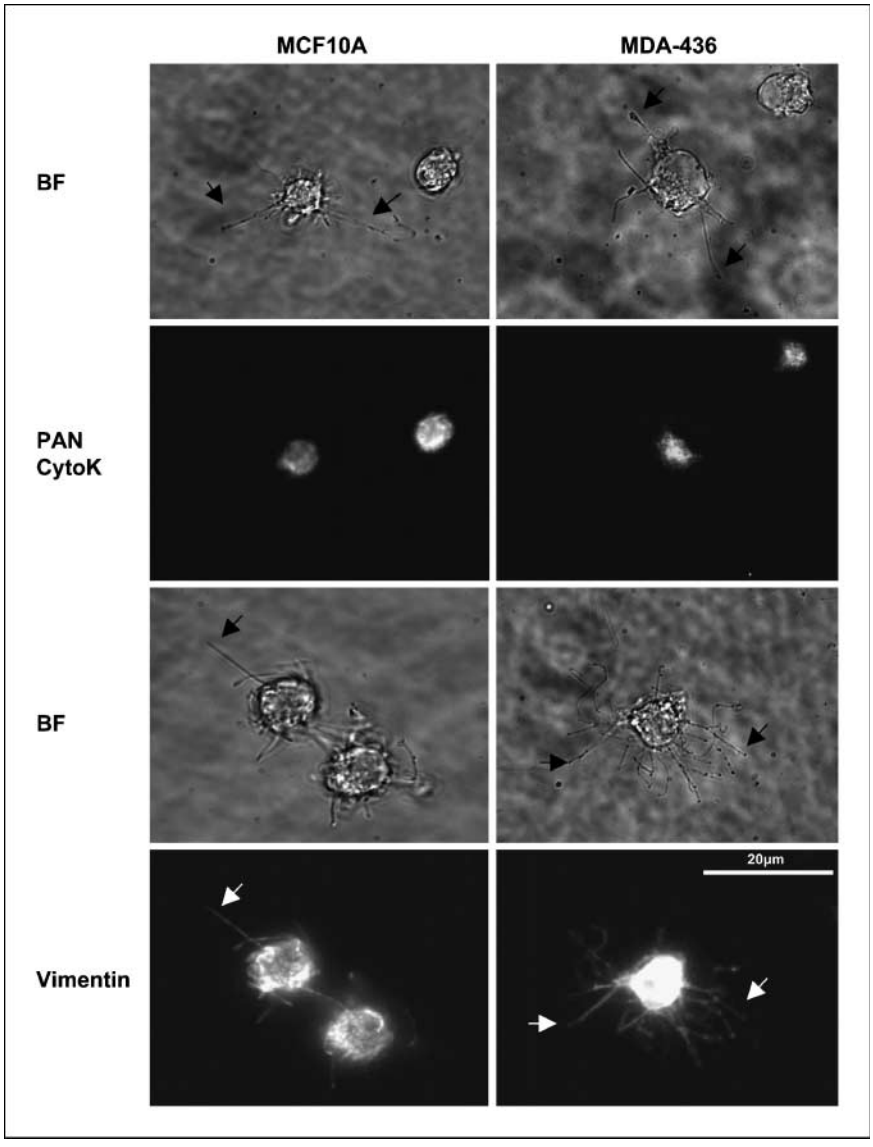

Figure 2. Vimentin, not cytokeratin, is localized to membrane microtentacles. MCF10A and MDA-436 were suspended for 30 min in media containing 5 μM LA. Cells were fixed in 0.5% glutaraldehyde while in suspension and gently spun onto glass coverslips coated with 1% PEI solution. Cells were fluorescently stained for vimentin or PAN cytokeratin (*CytoK*). Microtentacles stain positively for vimentin but not for cytokeratin. Microtentacles can be seen both by phase-contrast (*black arrow*) and fluorescence (*white arrow*).

MDA-MB-436 human carcinoma cell line and the fact that MCF10A cells express both cytokeratin and vimentin. Detached cells were fixed after 30 min in suspension in the presence or absence of 5 μM LA and centrifuged at low speed onto PEI-coated coverslips to preserve suspended cell architecture for immunofluorescence analysis. LA treatment enhanced the protrusive effect for immunofluorescence processing as previously described (10). Staining with antibodies against vimentin and a PAN cytokeratin reveal that vimentin is present in microtentacles whereas cytokeratin is limited to the cell body in MCF10A and weakly diffuse in MDA-MB-436 (Fig. 2). Subsequent immunofluorescence of preserved detached cells shows that vimentin and Glu-tubulin coalign in microtentacles of untreated and LA-treated cells, suggesting that vimentin may serve to reinforce Glu-tubulin in microtentacles (Fig. 3). Extension of microtentacles throughout three-dimensional space provides challenges to imaging, but confocal imaging allows exclusion of out-of-focus light in rounded cells and highlights the extension of vimentin in microtentacles (Fig. 3*B*).

Disruption of vimentin by phosphatase inhibitors decreases microtentacles. To determine effects of vimentin disruption on morphology and microtentacle frequency, we used two highly selective PP1/PP2A inhibitors that disassemble vimentin IFs via phosphorylation, OKA (1 μM) and Cal-A (5 nM; refs. 23, 24). MCF10A and MDA-MB-436 lose vimentin organization after treatment with OKA or Cal-A for 1 hour (Fig. 4*A*). Under normal growth conditions, MCF10A heterogeneously express vimentin in the cell population with intact vimentin extending to the cell periphery (Fig. 4*A, a*). MDA-MB-436 under normal growth conditions homogenously expresses vimentin that extends to the cell periphery with homogenous expression in the cell population (Fig. 4*A, e*). Both cell lines project vimentin filaments from a perinuclear region with concentrated vimentin. Cal-A treatment caused fragmentation and a decrease in vimentin that extended to the cell periphery in MCF10A (Fig. 4*A, b*), whereas a more pronounced effect in MDA-MB-436 was observed with cell rounding, vimentin fragmentation, and reorganization around the center of the cell body (Fig. 4*A, f*). Treatment with OKA resulted in a more dramatic change in vimentin morphology than Cal-A in MCF10A cells marked by cell rounding and vimentin fragmentation (Fig. 4*A, d*). MDA-MB-436 displayed similar morphologic changes with OKA as seen with Cal-A with a slight increase in retraction of the vimentin network to the perinuclear region (Fig. 4*A, h*). Control staining in the absence of serum did not cause noticeable effects on vimentin organization (Fig. 4*A, b* and *f*).

To exclude toxicity as a cause for vimentin disruption following Cal-A or OKA treatment, apoptosis was measured by PARP

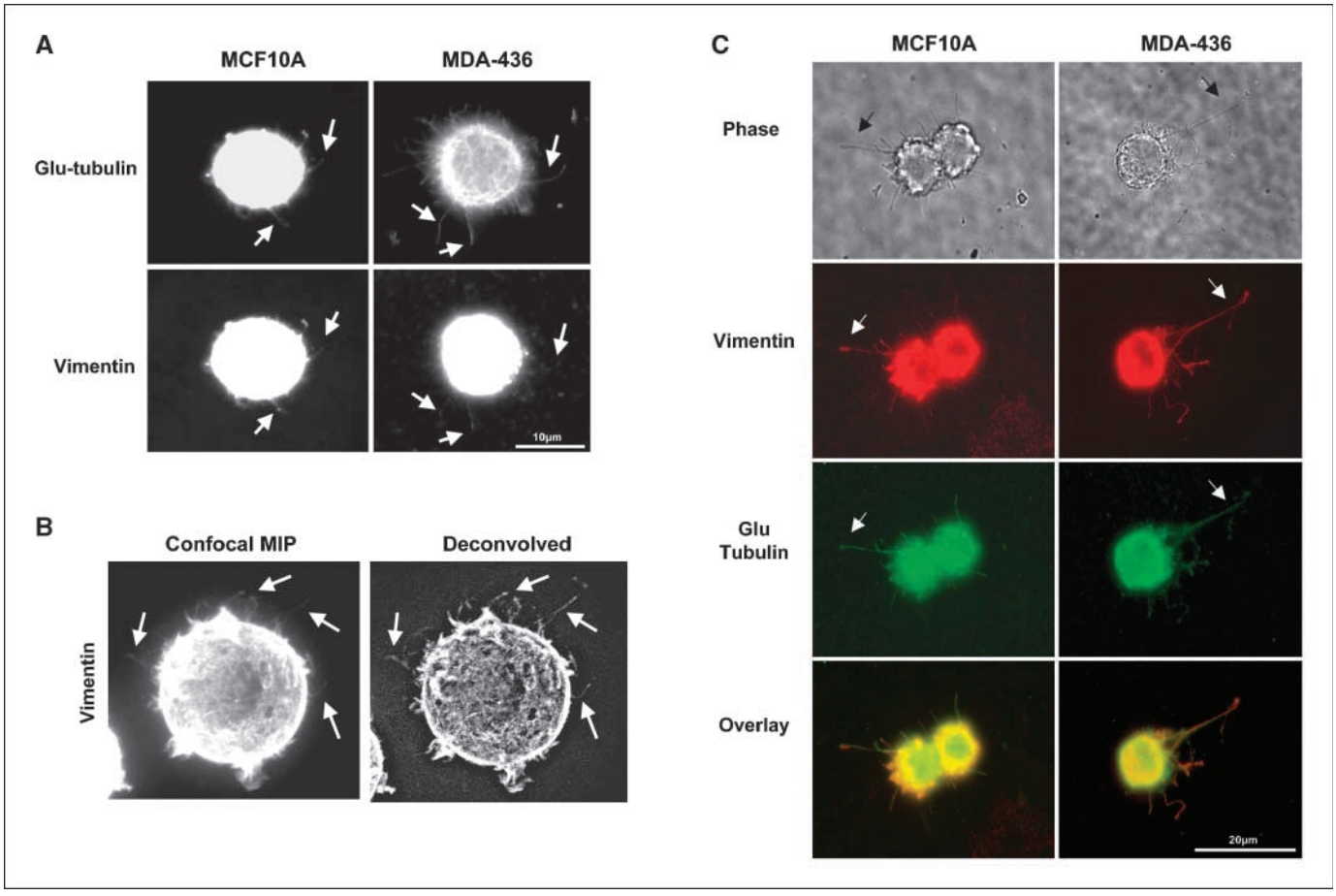

Figure 3. Vimentin aligns with Glu-tubulin in membrane microtentacles. MCF10A and MDA-436 were suspended for 30 min in DMEM (*A* and *B*) or media containing 5 μM LA (*C*). Cells were fixed in 0.5% glutaraldehyde while in suspension and gently spun onto glass coverslips coated with 1% PEI solution. *A,* immunostaining indicates that both vimentin and Glu-tubulin align in membrane microtentacles. *B,* a confocal maximum intensity projection (*MIP*) of an MDA-MB-436 cell computationally flattens the three-dimensional structure of the detached cell to allow visualization of microtentacles in different imaging planes. This image and one that has been deconvolved (Slidebook) show clear localization of vimentin in microtentacles (*arrows*). *C,* MDA-MB-436 display significantly longer microtentacles compared with MCF10A. Microtentacles can be seen both by phase-contrast (*black arrow*) and fluorescence (*white arrow*).

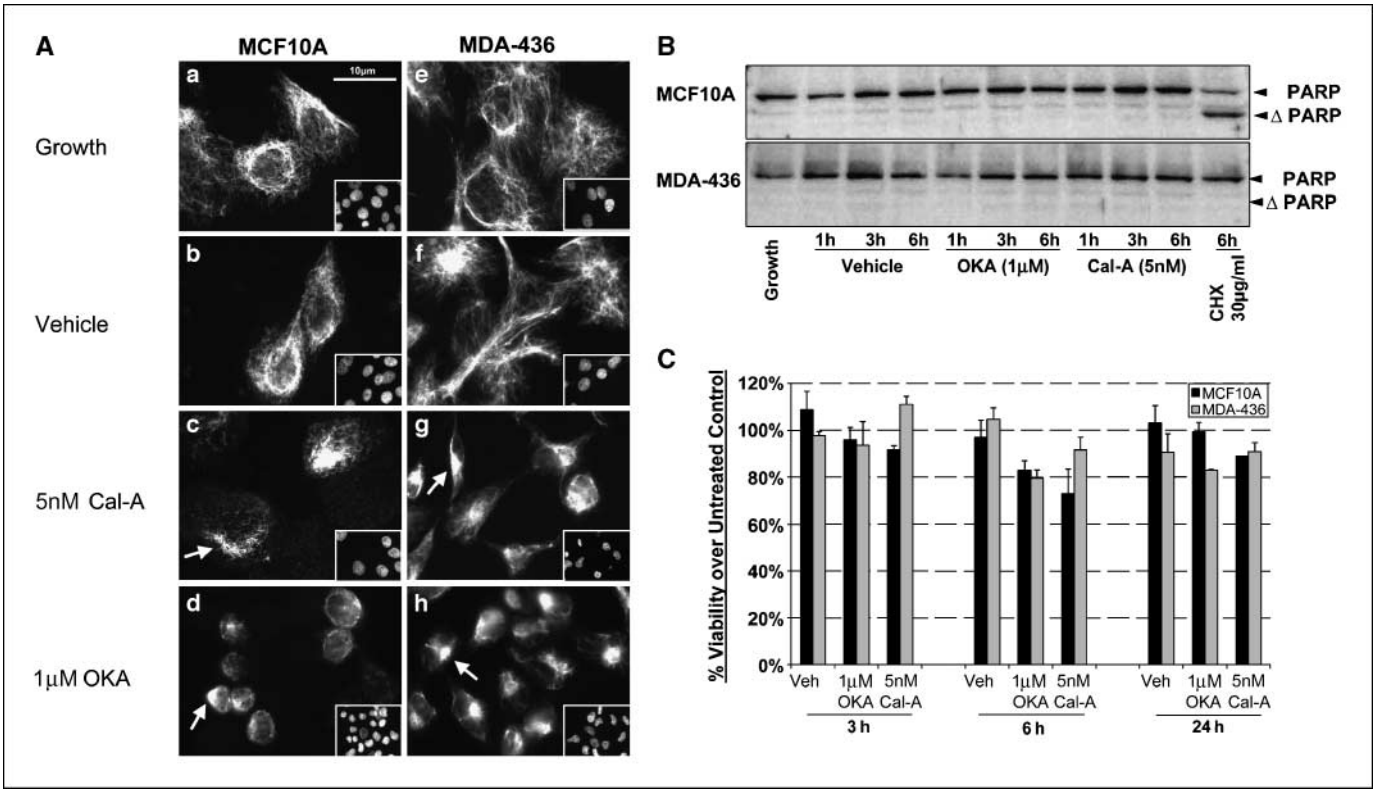

Figure 4. Inhibitors of PP1/PP2A disrupt vimentin without toxicity. Disruption of vimentin intermediate filaments following 1 h treatment in PP1/PP2A inhibitors is observed in attached MCF10A and MDA-MB-436 seeded on glass coverslips. *A,* MCF10A and MDA-MB-436 cells grown on glass coverslips were left untreated in growth media (*a* and *e*), vehicle (0.002% ethanol) treated in DMEM (*b* and *f*), 5 nM Cal-A (*c* and *g*), or 1 μM OKA (*d* and *h*). Vimentin is heterogeneously expressed in MCF10A while homogeneously expressed in MDA-MB-436 (inset depicts reference DNA stain). Treatment with PP1/PP2A inhibitors causes vimentin fragmentation and retraction to the perinuclear region compared with untreated and vehicle-treated cells (*white arrows*). *B,* cell lysates of MCF10A and MDA-MB-436 treated over for 1, 3, and 6 h in vehicle (0.002% ethanol), OKA (1 μM), Cal-A (5 nM), and positive control treatment cycloheximide (*CHX*, 30 μg/mL) were immunoblotted for PARP cleavage to show minimal degree of apoptosis caused by PP1/PP2A inhibitor treatment. PARP cleavage is observed in the MCF10A-positive control but no significant cleavage in presence of PP1/PP2A inhibitors. *C,* XTT viability assay shows minimal loss of cell viability via necrosis up to 24 h in presence of PP1/PP2A inhibitor treatment.

cleavage in MCF10A and MDA-MB-436 cells. No significant PARP cleavage occurred in either MCF10A and MDA-MB-436, even after 6 hours in Cal-A or OKA (Fig. 4*B*). MCF10A cells remain sensitive to cycloheximide-induced apoptosis, whereas MDA-MB-436 cells are resistant. An XTT viability assay was performed to confirm that the treatments did not cause apoptosis-independent cell death out to 24 hours (Fig. 4*C*).

GFP-Mem MCF10A and MDA-MB-436 were pretreated with either Cal-A or OKA for 1 hour to disrupt vimentin organization and then suspended in the presence of the corresponding pretreatment for 1 hour with or without the addition of LA. Blind microtentacle scoring in three independent trials showed a significant decrease in microtentacle frequency over the untreated control ($P < 0.05$, t test) following vimentin disruption by OKA and Cal-A (Fig. 5*A*) in both MCF10A and MDA-MB-436. LA-enhanced microtentacles are also significantly reduced by combination treatment with OKA + LA or Cal-A + LA ($P < 0.05$, t test).

Time-lapse DIC video microscopy shows that untreated MDA-MB-436 cells continue to produce active microtentacles when transiently attached to glass coverslips. The addition of either OKA or Cal-A reduced microtentacle motility and caused retraction ~30 minutes posttreatment (Fig. 5*B*; Supplementary Movies S7 and S8). These results further indicate that the stability and motion of microtentacles can be inhibited by compounds that affect vimentin phosphorylation.

Disruption of vimentin impairs attachment of vimentin-expressing cell lines. Given the role of micotentacles in the reattachment of suspended cells (10), we examined whether vimentin disruption with OKA and Cal-A would also affect reattachment. MCF10A and MDA-MB-436 were pretreated for 1 hour in OKA or Cal-A, then resuspended in same treatment over uncoated ($n = 3$) or laminin ($n = 3$) tissue culture plates, and assessed for cell reattachment. Plots of individual trials (conducted in triplicate) are represented in Fig. 5*C*, but the same trend was observed in all trials conducted (Supplementary Figs. S1 and S2).

While MCF10A attachment efficiency to either uncoated or laminin-coated surfaces was not significantly affected by Cal-A treatment, attachment was significantly sensitive to treatment with OKA (Fig. 6*A*). This result matches the less-pronounced vimentin disruption in MCF10A cells after Cal-A compared with OKA (Fig. 4*A, b* and *d*). Interestingly, MDA-MB-436 attachment was significantly impaired by the presence of either Cal-A or OKA (Fig. 5*C*). MDA-MB-436 attachment to uncoated surfaces was impaired (to a greater degree) more significantly at earlier time points (15 minutes to 3 hours) than over laminin at the same early time points. The delay in attachment of untreated MDA-MB-436 cells to laminin at early time points (15 minutes to 1.5 hours) compared with uncoated plates suggests that a possible adjustment time period is necessary for MDA-MB-436 cells to begin forming permanent attachments and spreading. Cells can become

independent of immobilized ECM coatings by depositing new ECM molecules, expressing different ECM receptors, or increasing the ECM receptors (25). Microtentacle-mediated reattachment of suspended cells to ECM *in vitro* (10) is therefore inhibited by compounds that affect vimentin assembly, and cells expressing high levels of vimentin, such as MDA-MB-436, are comparatively more sensitive to these compounds, potentially indicating a greater dependence of these cell lines on the expressed vimentin.

Dominant-negative vimentin mutant inhibits filament assembly and reduces microtentacles. To determine if vimentin directly supports the mechanism underlying microtentacles, we generated a dominant-negative vimentin mutant. With guidance

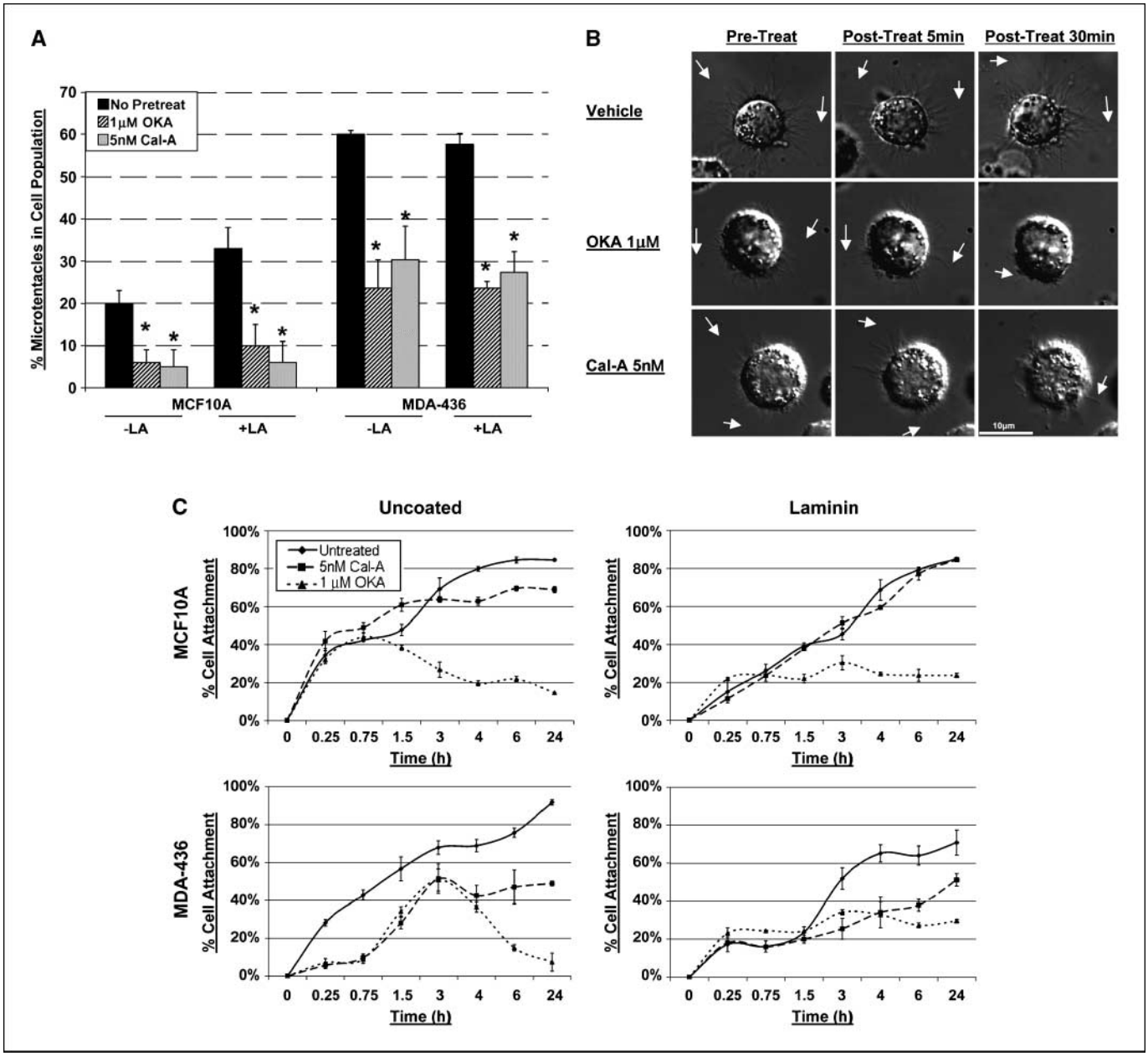

Figure 5. Vimentin disassembly with PP1/PP2A inhibitors reduces microtentacles and attachment. *A,* transiently transfected GFP-Mem MCF10A and MDA-MB-436 were left untreated (■) or pretreated for 1 h in OKA (1 μM, ▨) or Cal-A (5 nM, ▯) then suspended in DMEM ± LA (5 μM) in combination with respective pretreatment. Blind microtentacle counts were performed following 30-min suspension. *Bars,* mean + SD for three experiments in which at least 100 GFP-Mem$^+$ cells were counted. Pretreatment with both inhibitors and subsequent suspension in the same treatment show a statistically significant reduction in microtentacles in a cell population compared with the untreated counterpart ($P < 0.05$, *t* test, *black asterisks*). Suspension of cells in the presence of LA also show decrease in microtentacle frequency in combination with PP1/PP2A inhibitors ($P < 0.05$, *t* test, *black asterisks*). *B,* DIC time course of transiently attached MDA-MB-436 displaying motile membrane microtentacles captured over 30 min time course to observe effects of PP1/PP2A inhibitors on microtentacles (*white arrows*). *C,* disruption of vimentin by PP1/PP2A inhibitors affects cell attachment to surfaces. MCF10A and MDA-MB-436 were left untreated (-◆-) or pretreated for 1 h in Cal-A (5 nM, —■—) or OKA (1 μM, —▲—). Cells were detached and suspended over uncoated tissue culture plates or laminin-coated plates in the presence of the respective PP1/PP2A inhibitor pretreatment. Reattachment efficiency was measured by XTT viability at 24 h post-detachment. *Columns,* mean between triplicate wells of the percentage of cells attached in each well; *bars,* SD. Three independent experiments were performed showing similar attachment curves.

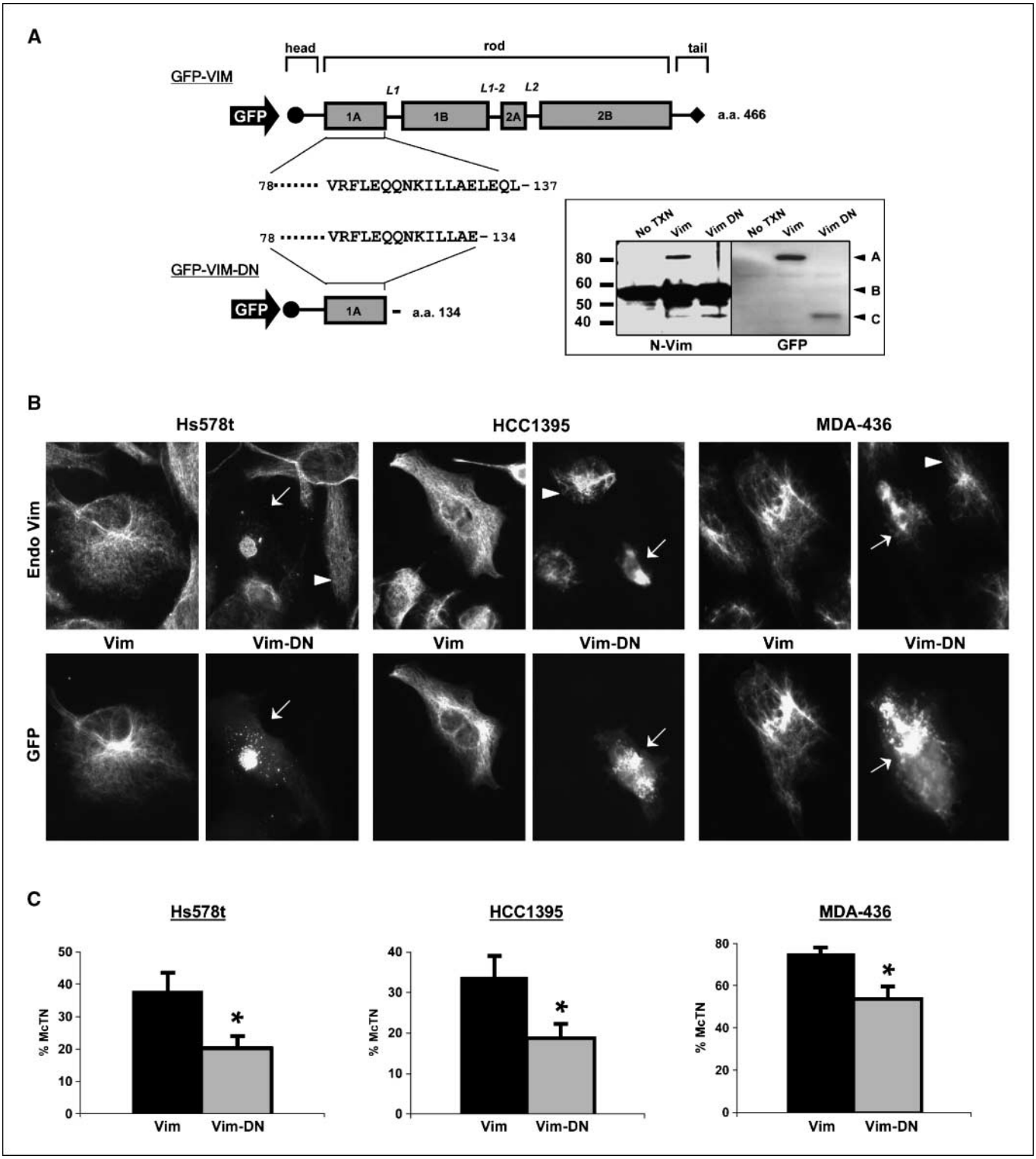

Figure 6. Dominant-negative vimentin (*Vim-DN*) disrupts filaments and reduces microtentacles. *A,* GFP-tagged human vimentin (*GFP-Vim*) was restricted with *Xho*I and religated with a unique *Xho*I site in the COOH terminal multiple cloning site to generate a dominant-negative form. The final Vim-DN construct preserves 134 a.a. of the full-length vimentin (466 a.a.) to include the head and highly conserved region of the rod 1A domain. Western blot analysis of Hs578t transfected with the GFP-Vim and GFP-Vim-DN indicates the expression of the truncated GFP-Vim-DN was recognized by both an NH_2 terminal vimentin antibody and GFP antibody. Inset: *A,* GFP Vim (85 kDa); *B,* Endo Vim (58 kDa); *C,* GFP-Vim-DN (43 kDa). *B,* vimentin-expressing cell lines (Hs578t, HCC1395, MDA-MB-436) were transfected with full-length vimentin (*GFP-Vim*) and dominant-negative (*GFP-Vim-DN*). Matched panels showing localization of the expressed protein (GFP) and endogenous vimentin (Endo Vim) indicate that GFP-Vim-DN disrupts endogenous vimentin in transfected cells (*white arrows*), whereas surrounding untransfected cells retain their IF network (*white arrowheads*). Expression of full-length GFP-Vim overlaid with the endogenous IF network indicates that the NH_2 terminal GFP tag Vim is not disruptive. *C,* cells cotransfected with GFP-Vim or GFP-Vim-DN and membrane-targeted RFP (*RFP-mem*) were suspended in DMEM, and blind microtentacle counts were performed following 30 min suspension. *Bars,* SD for at least three independent experiments in which a minimum of 100 RFP-Mem$^+$ cells were counted. Expression of the GFP-Vim-DN shows a statistically significant reduction in microtentacles compared with GFP-Vim transfection ($P < 0.001$, *t* test, *black asterisks*).

from studies of both *in vitro* vimentin assembly (26) and imaging of vimentin filaments in cells (27), we concluded that isolated expression of an amino-terminal fragment of vimentin lacking the tail region would effectively disrupt vimentin filaments. We engineered a stop codon at amino acid 134 of a GFP-vimentin expression vector, yielding a fragment (GFP-Vim-DN) that contains only the head domain of vimentin and a portion of the rod 1A domain but lacks any of the tail sequence that is essential for vimentin filament assembly (Fig. 6*A*). Both full-length GFP-vimentin and the GFP-Vim-DN fragment continue to be recognized by an amino-terminal vimentin antibody and GFP antibody, as well as displaying the expected molecular weight shift from fusion with GFP (Fig. 6*A, inset*). Expression of GFP-Vim-DN in three independent invasive breast tumor cell lines (Hs578t, HCC1395, and MDA-MB-436) disrupts endogenous vimentin filaments (Fig. 6*B*). Full-length GFP-vimentin integrates into filaments without disrupting endogenous vimentin. Cotransfection with a membrane-localized red fluorescent protein (pmRFP-Mem) allowed blinded microtentacle scoring in live cells and showed that GFP-Vim-DN significantly reduced microtentacle frequencies in each invasive cell line when compared with full-length GFP-Vim ($P < 0.001$, t test). Reducing vimentin expression with siRNA was not as effective as GFP-Vim-DN at reducing microtentacle frequencies. However, siRNA failed to fully eliminate vimentin, even after 6 days (Supplementary Fig. S3). Interestingly, blotting with a pan-intermediate filament antibody indicated that, as vimentin levels decreased, a new intermediate filament protein of ~65 kDa increased, suggesting a compensatory response to siRNA-mediated vimentin reduction. Such a compensatory mechanism has been proposed for why vimentin knockout mice are viable and phenotypically normal (28) and illustrates the potential limitations of siRNA-mediated down-regulation of such an abundant gene with numerous redundant family members. Nevertheless, expression of GFP-Vim-DN disrupted endogenous vimentin filaments within 1 day and provides genetic evidence that vimentin directly supports the molecular mechanism underlying microtentacles in detached breast tumor cells.

Discussion

Cytoskeletal rearrangements, release of cell-cell contacts, and loss of organized tissue architecture are hallmarks of metastatic progression (29). We previously reported that detached mammary epithelial cells display novel membrane protrusions enriched in detyrosinated α-tubulin, which we have termed tubulin *microtentacles* (10). Continuing our investigation into the occurrence of such microtentacles using a panel of breast carcinoma cells has revealed a marked increase in both microtentacle extension and frequency in more invasive tumor lines. Our data showing colocalization of vimentin with Glu-tubulin in microtentacles, the extensive microtentacles formed in cells with high vimentin expression, and the inhibition of microtentacles with dominant-negative vimentin or compounds targeting vimentin assembly, all support a model in which structural coordination of Glu-tubulin and vimentin underlie the striking morphologic abnormalities we observe in detached breast tumor cells.

Our data also indicate that microtentacles in detached cells are distinct from other actin-based structures in attached cells, such as invadopodia or podosomes (30), which are inhibited by actin-destablizing agents, such as LA or Cytochalasin-D. In contrast, microtentacles are enhanced by actin disruption and seem to become more flexible, motile, and longer (Fig. 1*B*). This supports a model in which inward contraction of the cortical actin of the cell counteracts the mechanical forces exerted outward by filaments such as microtubules and vimentin, and we are currently examining this repressive role for cortical actin in detail.[3] Microtubule-based cilia are characteristically shorter and more highly organized. In addition, microtubule-based cilia are not known to depend on intermediate filament proteins and their characteristic beat remains unaffected by concentrations of okadaic acid that exceed those we used in our study (31). However, it is possible that tubulin microtentacles were mistakenly identified as such classic cytoskeletal structures in the past. Interestingly, a patient case study reported the occurrence of multiple, "abnormal" microtubule protrusions in an infiltrating mammary ductal carcinoma but remains uncharacterized (32).

Vimentin expression is a marker of the aggressive "basal cell" subtype of breast tumor (33, 34), and up-regulation of vimentin predicts metastatic progression and poor patient prognosis (35). Beyond breast cancer, vimentin is an established independent predictor of poor patient prognosis in many tumors, including cervical (36), thyroid (37), hepatocellular (38), pancreatic (39), and renal carcinomas (40). Our results indicate that cell lines with the highest microtentacle counts display reduced expression of cytokeratins and increased vimentin, a change which is also observed during the epithelial-to-mesenchymal transition (EMT) that is associated with tumor progression and poor patient prognosis (41, 42). Interestingly, vimentin is also strongly up-regulated when tumor cells are exposed to hypoxia (43). Our current evidence supports a direct role for vimentin in the mechanism underlying microtentacles in detached breast tumor cells. Determining how this role for vimentin relates to the additional phenotypic and transcriptional changes that occur during EMT and hypoxia will certainly be an important focus in future studies. In this report, we primarily consider how physical properties of vimentin could support microtentacle extension and potentially provide a selective advantage to tumor cells during metastasis.

Vimentin filaments are far more resilient than microtubules and play an important role in maintaining the integrity and morphology of fibroblastic cells (44). Despite its stability, vimentin can rapidly reorganize in response to phosphorylation. Live cell imaging indicates that microtentacles are composed of cytoskeletal elements with the structural stability to persist in suspension yet also remain dynamic enough to support rapid movement in response to the cellular microenvironment (Figs. 1 and 5 and Supplementary Movies). Phosphatases associated with vimentin promote filament stability and regulate binding ability to IF-associated proteins, such as microtubules (45). Furthermore, vimentin is rapidly hyperphosphorylated and disassembled after treatment with specific inhibitors of types 1 and 2A phosphatases, providing evidence that vimentin is a major target of PP1 and PP2A activity (23, 24).

There is strong evidence that vimentin and stabilized microtubules are connected via shared associated proteins, such as kinesin motor proteins (46), microtubule-associated proteins, and intermediate filament associated proteins. Ongoing investigation in our laboratory indicates that kinesins are involved in the

[3] E.M. Balzer et al., submitted manuscript.

microtentacle motility when cells are detached.[4] Kinesin-dependent cross-linking with vimentin could reinforce stabilized microtubules to allow the plasma membrane deformations that we observe during microtentacle extension. Contraction of the network of cortical actin filaments that lie beneath the plasma membrane usually provides an inward force that counteracts the outward expansion of microtubules from the cell center. The resulting balance of actin and microtubule forces stabilizes cells and is termed tensegrity (47). The actin cortex may therefore provide a physical barrier to microtubules, which are relatively easily broken when encountering compressive stress (48). However, tension and rigidity in the actin cortex decrease when cells are detached, which may partially remove this barrier (49). In addition, compelling recent studies trapping detached breast tumor cells with optical tweezers shows that cell lines with higher metastatic potential have greater flexibility in their actin cortex (50). This inherent weakness in the actin cortex of metastatic breast tumor cells may explain the greater microtentacle extension of invasive breast tumor cell lines, even without actin depolymerization (Fig. 1). Given the interest in cytoskeletally directed therapies for breast cancer, we are currently examining how the counteracting forces of stabilized microtubules and the actin cortex regulate microtentacle extension in breast tumor cells.[5]

Based on our results, we propose that, upon detachment, vimentin aligns with stable microtubules via associated proteins to provide a flexible scaffold to Glu-enriched microtubules, which allows microtentacles to protrude at great length from the cell body. The shorter, less frequent microtentacles observed in non–vimentin-expressing, less invasive cell lines likely rely on the population of stable microtubules but lack the increased resilience and strength of vimentin filaments (48). Disruption of vimentin filaments with either PP1/PP2A inhibitors or dominant-negative mutant vimentin likely promotes the collapse of Glu-microtubules and ultimate deformation of the microtentacles.

Research models that involve studying attached cells in culture have limitations when investigating critical steps in the process of metastasis. While we continue to pursue the functional role of tubulin microtentacles in metastasis, the dramatic morphologic differences observed in detached breast tumor cell lines are compelling. Intriguing *in vivo* evidence exists that a yet-unidentified, tubulin-based (*not* actin-based) mechanism promotes the binding of circulating tumor cells to the vascular endothelium (11). It will therefore be important to determine whether the increased microtentacles in metastatic breast tumor cell lines provide an advantage for successful reattachment and extravasation following dissemination from the primary tumor site. A greater understanding of the foundation and activity of such extensive tubulin microtentacles displayed by invasive carcinoma cells may present an intriguing new target for cancer therapy.

[4] J. Yoon et al., manuscript in preparation.
[5] E.M. Balzer et al., submitted manuscript.

Disclosure of Potential Conflicts of Interest

No potential conflicts of interest were disclosed.

Acknowledgments

Received 12/12/2007; revised 4/11/2008; accepted 5/12/2008.

Grant support: Howard Temin career award K01-CA096555 and 1R01CA124704-01 from National Cancer Institute, Breast Cancer Idea award BC061047 from USA Medical Research and Material Command, and Cigarette Restitution Fund Cancer Research grant CH 649 CRF from State of Maryland Department of Health and Mental Hygiene.

The costs of publication of this article were defrayed in part by the payment of page charges. This article must therefore be hereby marked *advertisement* in accordance with 18 U.S.C. Section 1734 solely to indicate this fact.

We thank Georges Lutfalla for kindly sharing the membrane-localized RFP expression vector.

References

1. Steeg PS. Tumor metastasis: mechanistic insights and clinical challenges. Nat Med 2006;12:895–904.
2. Wittekind C, Neid M. Cancer invasion and metastasis. Oncology 2005;69 Suppl 1:14–6.
3. Gupta GP, Massague J. Cancer metastasis: building a framework. Cell 2006;127:679–95.
4. Wolf K, Friedl P. Molecular mechanisms of cancer cell invasion and plasticity. Br J Dermatol 2006;154 Suppl 1: 11–5.
5. Yamauchi K, Yang M, Jiang P, et al. Real-time *in vivo* dual-color imaging of intracapillary cancer cell and nucleus deformation and migration. Cancer Res 2005;65: 4246–52.
6. Tsuji K, Yamauchi K, Yang M, et al. Dual-color imaging of nuclear-cytoplasmic dynamics, viability, and proliferation of cancer cells in the portal vein area. Cancer Res 2006;66:303–6.
7. Martin SS, Vuori K. Regulation of Bcl-2 proteins during anoikis and amorphosis. Biochim Biophys Acta 2004; 1692:145–57.
8. Martin SS, Ridgeway AG, Pinkas J, et al. A cytoskeleton-based functional genetic screen identifies Bcl-xL as an enhancer of metastasis, but not primary tumor growth. Oncogene 2004;23:4641–5.
9. Martin SS, Leder P. Human MCF10A mammary epithelial cells undergo apoptosis following actin depolymerization that is independent of attachment and rescued by Bcl-2. Mol Cell Biol 2001;21:6529–36.
10. Whipple RA, Cheung AM, Martin SS. Detyrosinated microtubule protrusions in suspended mammary epithelial cells promote reattachment. Exp Cell Res 2007; 313:1326–36.
11. Korb T, Schluter K, Enns A, et al. Integrity of actin fibers and microtubules influences metastatic tumor cell adhesion. Exp Cell Res 2004;299:236–47.
12. Barra HS, Arce CA, Argarana CE. Posttranslational tyrosination/detyrosination of tubulin. Mol Neurobiol 1988;2:133–53.
13. Webster DR, Gundersen GG, Bulinski JC, Borisy GG. Assembly and turnover of detyrosinated tubulin *in vivo*. J Cell Biol 1987;105:265–76.
14. Mialhe A, Lafanechere L, Treilleux I, et al. Tubulin detyrosination is a frequent occurrence in breast cancers of poor prognosis. Cancer Res 2001;61:5024–7.
15. Kato C, Miyazaki K, Nakagawa A, et al. Low expression of human tubulin tyrosine ligase and suppressed tubulin tyrosination/detyrosination cycle are associated with impaired neuronal differentiation in neuroblastomas with poor prognosis. Int J Cancer 2004;112:365–75.
16. Soucek K, Kamaid A, Phung AD, et al. Normal and prostate cancer cells display distinct molecular profiles of α-tubulin posttranslational modifications. Prostate 2006;66:954–65.
17. Khawaja S, Gundersen GG, Bulinski JC. Enhanced stability of microtubules enriched in detyrosinated tubulin is not a direct function of detyrosination level. J Cell Biol 1988;106:141–9.
18. Gurland G, Gundersen GG. Stable, detyrosinated microtubules function to localize vimentin intermediate filaments in fibroblasts. J Cell Biol 1995;131:1275–90.
19. Yoon M, Moir RD, Prahlad V, Goldman RD. Motile properties of vimentin intermediate filament networks in living cells. J Cell Biol 1998;143:147–57.
20. Ball EH, Singer SJ. Association of microtubules and intermediate filaments in normal fibroblasts and its disruption upon transformation by a temperature-sensitive mutant of *Rous sarcoma* virus. Proc Natl Acad Sci U S A 1981;78:6986–90.
21. Pruss RM, Mirsky R, Raff MC, Thorpe R, Dowding AJ, Anderton BH. All classes of intermediate filaments share a common antigenic determinant defined by a monoclonal antibody. Cell 1981;27:419–28.
22. Campbell RE, Tour O, Palmer AE, et al. A monomeric red fluorescent protein. Proc Natl Acad Sci U S A 2002; 99:7877–82.
23. Eriksson JE, He T, Trejo-Skalli AV, et al. Specific *in vivo* phosphorylation sites determine the assembly dynamics of vimentin intermediate filaments. J Cell Sci 2004;117:919–32.
24. Lee WC, Yu JS, Yang SD, Lai YK. Reversible hyperphosphorylation and reorganization of vimentin intermediate filaments by okadaic acid in 9L rat brain tumor cells. J Cell Biochem 1992;49:378–93.
25. Mooney DJ, Langer R, Ingber DE. Cytoskeletal filament assembly and the control of cell spreading and function by extracellular matrix. J Cell Sci 1995;108: 2311–20.
26. Traub P, Scherbarth A, Wiegers W, Shoeman RL. Salt-stable interaction of the amino-terminal head region of vimentin with the α-helical rod domain of cytoplasmic intermediate filament proteins and its relevance to protofilament structure and filament formation and stability. J Cell Sci 1992;101:363–81.

27. McCormick MB, Kouklis P, Syder A, Fuchs E. The roles of the rod end and the tail in vimentin IF assembly and IF network formation. J Cell Biol 1993;122:395–407.

28. Moisan E, Chiasson S, Girard D. The intriguing normal acute inflammatory response in mice lacking vimentin. Clin Exp Immunol 2007;150:158–68.

29. Gotzmann J, Mikula M, Eger A, et al. Molecular aspects of epithelial cell plasticity: implications for local tumor invasion and metastasis. Mutat Res 2004;566: 9–20.

30. Yamaguchi H, Pixley F, Condeelis J. Invadopodia and podosomes in tumor invasion. Eur J Cell Biol 2006;85: 213–8.

31. Sutto Z, Conner GE, Salathe M. Regulation of human airway ciliary beat frequency by intracellular pH. J Physiol 2004;560:519–32.

32. Reilova-Velez J, Seiler MW. Abnormal cilia in a breast carcinoma. An ultrastructural study. Arch Pathol Lab Med 1984;108:795–7.

33. Rodriguez-Pinilla SM, Sarrio D, Honrado E, et al. Vimentin and laminin expression is associated with basal-like phenotype in both sporadic and BRCA1-associated breast carcinomas. J Clin Pathol 2006;60: 1006–12.

34. Rakha EA, El-Rehim DA, Paish C, et al. Basal phenotype identifies a poor prognostic subgroup of breast cancer of clinical importance. Eur J Cancer 2006; 42:3149–56.

35. Domagala W, Striker G, Szadowska A, Dukowicz A, Harezga B, Osborn M. p53 protein and vimentin in invasive ductal NOS breast carcinoma-relationship with survival and sites of metastases. Eur J Cancer 1994;30A: 1527–34.

36. Gilles C, Polette M, Piette J, et al. Vimentin expression in cervical carcinomas: association with invasive and migratory potential. J Pathol 1996;180:175–80.

37. Vasko V, Espinosa AV, Scouten W, et al. Gene expression and functional evidence of epithelial-to-mesenchymal transition in papillary thyroid carcinoma invasion. Proc Natl Acad Sci U S A 2007;104:2803–8.

38. Hu L, Lau SH, Tzang CH, et al. Association of vimentin overexpression and hepatocellular carcinoma metastasis. Oncogene 2004;23:298–302.

39. Javle MM, Gibbs JF, Iwata KK, et al. Epithelial-mesenchymal transition (EMT) and activated extracellular signal-regulated kinase (p-Erk) in surgically resected pancreatic cancer. Ann Surg Oncol 2007;14: 3527–33.

40. Kim HL, Seligson D, Liu X, et al. Using tumor markers to predict the survival of patients with metastatic renal cell carcinoma. J Urol 2005;173:1496–501.

41. Domagala W, Lasota J, Dukowicz A, et al. Vimentin expression appears to be associated with poor prognosis in node-negative ductal NOS breast carcinomas. Am J Pathol 1990;137:1299–304.

42. Willipinski-Stapelfeldt B, Riethdorf S, Assmann V, et al. Changes in cytoskeletal protein composition indicative of an epithelial-mesenchymal transition in human micrometastatic and primary breast carcinoma cells. Clin Cancer Res 2005;11:8006–14.

43. Krishnamachary B, Berg-Dixon S, Kelly B, et al. Regulation of colon carcinoma cell invasion by hypoxia-inducible factor 1. Cancer Res 2003;63:1138–43.

44. Goldman RD, Khuon S, Chou YH, Opal P, Steinert PM. The function of intermediate filaments in cell shape and cytoskeletal integrity. J Cell Biol 1996;134: 971–83.

45. Inagaki M, Nishi Y, Nishizawa K, Matsuyama M, Sato C. Site-specific phosphorylation induces disassembly of vimentin filaments *in vitro*. Nature 1987;328: 649–52.

46. Prahlad V, Yoon M, Moir RD, Vale RD, Goldman RD. Rapid movements of vimentin on microtubule tracks: kinesin-dependent assembly of intermediate filament networks. J Cell Biol 1998;143:159–70.

47. Ingber DE. Tensegrity II. How structural networks influence cellular information processing networks. J Cell Sci 2003;116:1397–408.

48. Janmey PA, Euteneuer U, Traub P, Schliwa M. Viscoelastic properties of vimentin compared with other filamentous biopolymer networks. J Cell Biol 1991;113:155–60.

49. Heidemann SR, Kaech S, Buxbaum RE, Matus A. Direct observations of the mechanical behaviors of the cytoskeleton in living fibroblasts. J Cell Biol 1999;145: 109–22.

50. Guck J, Schinkinger S, Lincoln B, et al. Optical deformability as an inherent cell marker for testing malignant transformation and metastatic competence. Biophys J 2005;88:3689–98.